Downstream evolution of the Bénard–von Kármán instability

S. Goujon-Durand*, P. Jenffer,† and J.E. Wesfreid
Laboratoire d'Hydrodynamique et Mécanique Physique (URA CNRS No. 857), Ecole Supérieure de Physique et Chimie Industrielles de Paris, 10, rue Vauquelin, 75231 Paris Cedex 05, France
(Received 28 October 1993)

We describe experiments in the Bénard–von Kármán hydrodynamic instability of the vortex shedding behind an obstacle. We obtain the scaling laws for the evolution of the global mode describing the envelope of the peak to peak amplitude velocity oscillation of the flow velocity and we show the existence of a universal curve for the renormalized amplitude of the streamwise evolution of this amplitude.

PACS number(s): 47.20.Ky, 47.27.Vf, 47.15.Fe

I. INTRODUCTION

We analyze experimental results on the streamwise evolution of the vortex shedding in the flow behind an obstacle (Bénard–von Kármán instability). Kovasznay [1] has performed a complete study of the spatial properties of the vortex shedding and has analyzed the downstream evolution of the amplitude of the peak to peak oscillation (envelope) of the fluid velocity measured with hot wires in the central line. He observed that this amplitude grows far away from the obstacle and has a maximum near $x = 7d$, with d the diameter of the cylindrical obstacle, and afterwards decreases in the flow direction.

In 1983 Mathis [2] showed preliminary results where he detected that this maximum position changed with the Reynolds number and became larger than $5d$ when the flow velocity approached the critical Reynolds number R_c at the onset of shedding. This observation suggests to us a critical behavior of this envelope as is the case in confined hydrodynamic instabilities such as Rayleigh-Bénard convection [3].

The spatial properties of the vortex shedding were studied with the concept of a global mode of instability in open systems with spatially developing flows [4–9]. As is now very well known [10,11], the wake instability is absolutely unstable downstream near the bluff body and convectively unstable far away. The synchronized oscillation of the shedding instability in all the flow domain is characteristic of the existence of a global mode.

The spatially developed base flow induced by the obstacle in front of the incoming flow shows different local stability along this direction [12] and this can be modeled by a decreasing relative Reynolds number $\varepsilon = \varepsilon(x)$, where $\varepsilon = (R - R_c)/R_c$. The first theoretical studies to calculate the form of the global mode were using a linear Landau equation as a model for the amplitude of the eigenfunction in the stream direction x [4]. The envelope solutions obtained are Airy functions when $\varepsilon(x)$ is linearly decreasing and parabolic cylinder functions when $\varepsilon(x)$ is quadratically decreasing [13]. The experimental test of these models and the quantitative study of global modes still remain open.

In order to observe these global modes and their evolution as functions of the Reynolds number we have performed experiments to measure the amplitude of the velocity perturbations in the central line of the flow behind the obstacle for supercritical Reynolds numbers when vortex shedding takes place. Our experiments were done in a low velocity water tunnel where the velocity was measured with a laser Doppler anemometer (LDA). The bluff body is of trapezoidal form to ensure straight corners and a constant initial spatial phase to the vortex shedding is defined. This shape, more efficient than in the classical cylindrical shape, is normally used in industrial flowmeters in order to ensure more stable and robust vortex emission [14].

The study that we present here is complementary and different from the study of the spatial properties of the vortex emission along the body direction z. This problem has already been observed and discussed extensively. Indeed comprehensive work was done in order to understand the influence of the sidewalls, the existence of chevrons, the shedding of inhomogeneous obstacles, etc., and almost all the situations are very well modeled by Landau-Ginzburg models including the spatial derivatives in function of the coordinate z [15–17].

II. EXPERIMENTAL SETUP

Our experiments were performed in a low velocity water tunnel with typical velocities of 1–2 cm/sec at the onset of instability. The bluff body of trapezoidal section (Fig. 1) is characterized by its width d. We have used $d = 1$, 0.5, and 0.4 cm in different experiments. The angle of the lateral faces is 4° and the ratio of the length l of the long side of the trapeze in the upstream face, to the width d, is $l/d = 0.7$. The transverse extension of

*Also at Laboratoire d'Electronique, Université Paris XII Val de Marne, Créteil, France.
†Also at Université Paris Sud, Orsay, France.

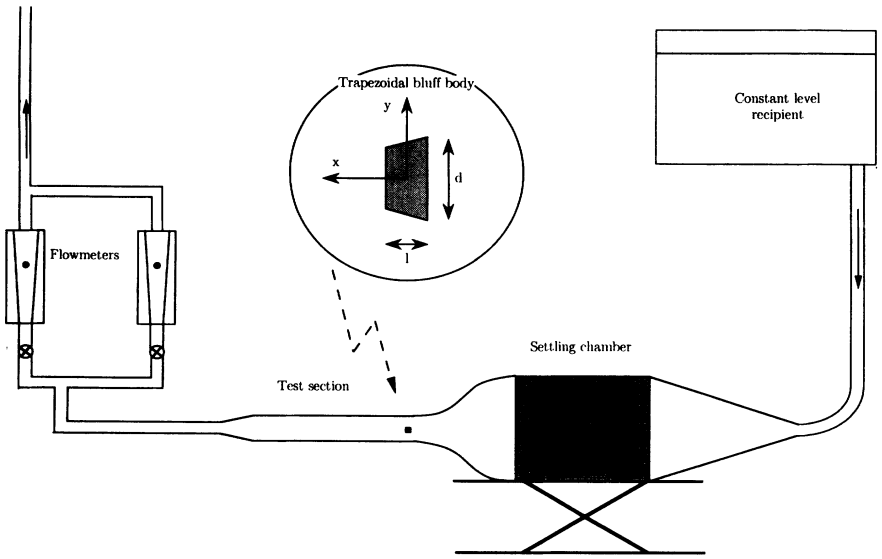

FIG. 1. Experimental setup.

the body (L_z) is 5 cm.

The channel has a square section of 5×5 cm^2 and is preceded by a settling chamber and a convergent. A LDA scans the transverse (V_x) and longitudinal velocities (V_y) from the center of the bluff body (it is the x origin) until $x = 10$ cm downstream. The velocity value is obtained by processing the Doppler bursts with a frequency counter and this instantaneous velocity value is analyzed by a fast Fourier transform (FFT) analyzer in order to obtain the frequency of the shedding and its amplitude. The flow in the channel is achieved gravitationally by a constant head pressure, and exit gates modify the flow rate.

In the central line (at $y = 0$) the longitudinal component of the velocity has a special dynamics behavior. Indeed, for the shedding frequency f_0, the V_x component of the velocity fluctuation shows the presence of the harmonic $2f_0$. In fact Kovasznay [1] noticed that this component can be written as

$$V_x = V_1 \cos 2\pi(\zeta_1 + f_0 t) + V_2 \cos 2\pi(\zeta_2 + 2f_0 t), \quad (1)$$

where V_1 is an odd function of y. As the velocity probe senses the synchronized upper and lower vortex emission, when it is nearer one of the trails ($y \neq 0$) it senses essentially its contribution at frequency f_0. But the transverse component V_y always shows the f_0 frequency. In our experiments we observed, for the transverse component V_y in the central line, the harmonic $2f_0$, as our LDA system does not determine the sign of the velocity component and the frequency counter dressed the velocity signal. In order to take into account these situations we recorded the values of the amplitude of each mode and the total power spectrum in the FFT analyzer.

They are two dye (fluorescein) injectors in the bluff body. With an ion argon laser light sheet produced by a cylindrical lens we are able to visualize the eddies by laser induced fluorescence (LIF) and check the two-dimensional structure of the shedding.

III. EXPERIMENTAL RESULTS

We have measured the transverse V_y component of the velocity and we have explored the oscillating downstream velocity field, from the obstacle (at $x = d/2$) to $x = 10$ cm in the central line at $y = 0$ (it is $x = 10d$, $x = 20d$, and $x = 25d$ for the different obstacles). These measurements were done for numerous Reynolds numbers ranging from R_c to $2R_c$, where R_c is the onset of the Hopf bifurcation in the absolute regime of instability. We have chosen the V_y component of the velocity oscillation. This component of the flow velocity is zero when $R < R_c$ and reaches a maximum in the symmetric central line [1]. The V_x component of the velocity fluctuation is not maximal in the central line; it is maximal for a certain $y = y_{max}$ [18] and we are not able to ensure then that this y_{max} value does not change when the Reynolds number is modified.

In Fig. 2(a) we show the visualization image obtained by LIF visualization, where the instantaneous view of the streak lines is superposed with the average view during many periods. In Fig. 2(b), at the same spatial scale, we display the evolution of the envelope of the peak to peak amplitude, from the velocity measurements.

We can observe that the strength of the emission grows after the obstacle reaches a maximal value (around $x = 4d$ in the figure) and decays downstream, as was noticed by Kovasznay [1] and Mathis [2]. We can notice that the streak lines of the dye visualization do not show [19] this important feature of the spatial development and we observe a strong discrepancy between the "tracer envelope," obtained by dye visualization in Fig. 2(a), and the velocity envelope in Fig. 2(b).

The physical origin of this downstream decay is the viscous relaxation of the shear base profile induced behind the bluff body. This relaxation reduces the strength of the local relative Reynolds number $\varepsilon(x)$. This instability parameter becomes negative far away from the origin in bluff body. This downstream relaxation of the shedding oscillation is one of the typical characteristics of open flow instabilities with spatial inhomogeneity [5].

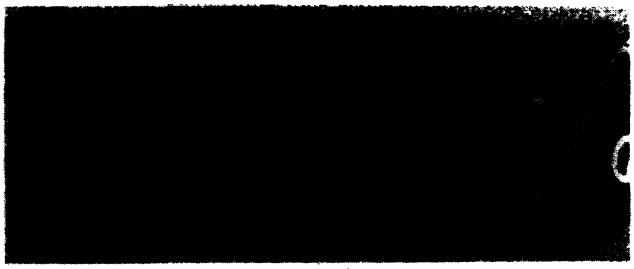

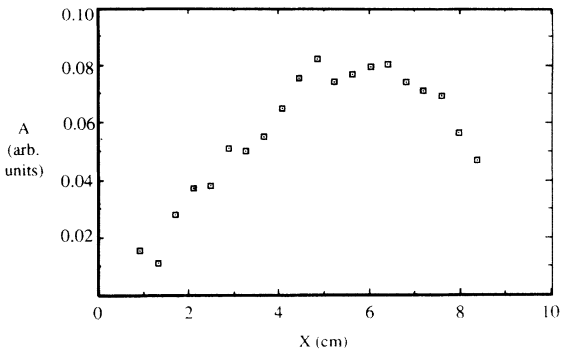

FIG. 2. (a) Laser induced fluorescence view of vortex emission. The picture shows the superposition of an instantaneous view of the streak line and the time averaged streak lines during many periods. (b) Normalized maximum amplitude of the transversal fluctuation of velocity along the x streamwise direction, measured with laser Doppler anemometry.

In order to appreciate this relaxation, we have performed measurements of the V_x (longitudinal component of the flow velocity) at different x locations of the water channel and for all the values of y (the transverse coordinate) at $z = 0$ (in the middle of the channel), at a Reynolds number just before the onset of instability. We observe a strong variation of this base flow profile in the downstream direction. This in turn leads to a reduction of the strength of the instability due to the downstream relaxation of the base flow.

The variation of the spatial scale of the base flow (equivalent to the boundary layer thickness δ) induced a nonparallel flow, as can be deduced from the continuity equations. The systematic exploration of the full velocity field can give us the value of the degree of the nonparallelism parameter.

From measurements obtained after careful exploration of the velocity field, we obtained the envelope of the peak to peak amplitude as shown in Fig. 2(b). We repeated these explorations for different Reynolds numbers and obtained the results shown in Fig. 3. In this figure we plotted the total power of the frequency spectrum containing the information of the highest peak at $f = 2f_0$.

The alternative way to plot these results was by considering that only the highest peak are less coherent with the plots including total power.

At the same time we obtained the value of the frequency on each x and we observe that this value was constant within the error limits along the flow direction. This constant frequency implies a synchronized oscillation and is one of the major features of the existence of a global instability in the full domain of shedding. Experiments are in progress to complete this description with local measurements of the growth rate of perturbations in order to compare the behavior of the imaginary part of the growth rate ($\omega_i = f$, the frequency of oscillation) to the real part of this rate ω_r, giving the amplification of the instability. From the measurement of the frequency f_0 we obtain the plot shown in Fig. 4, which is a representation of the Strouhal law showing that the frequency of shedding increases linearly with the Reynolds number, from the value f_{0c} at the onset of the Hopf bifurcation. We completed this description with measurements of the frequency in the subcritical region $R < R_c$ when an external abrupt perturbation of the flow is introduced upstream in the flow and we can observe the transitory decaying vortex emission stimulated by the perturbation, as done before by Provensal *et al.* [20].

The slope of the curve frequency vs Reynolds number gives the imaginary part of the complex coefficients $(c_0 - c_2)$ in the Landau model description of this instability [20,21] and the slope in the subcritical region gives the linear coefficient c_0. Our measurements give an estimate of $c_2/c_0 \approx -0.2$ [22].

One of the original aspects of these measurements is an encouraging confirmation of the tendency observed in the preliminary results of Mathis [2] about the Reynolds dependence in the location of the maximum in amplitude, called X_{max}. We observed that in our experiments this value was shifting far away from the bluff body when we approached the onset R_c. From these measurements we could observe that a dependence in the Reynolds number begins to be suggested. From the log-log plot of Fig. 5 we proposed a law in $X_{max} \sim (R - R_c)^{-1/2}$ as a reasonable fit to our measurements.

Let us look at the validity of the result of Fig. 5. Indeed, when $R \to R_c$, the maximum of the amplitude oscillation approaches zero and from the experimental point of view it is very difficult to establish precisely the position of the maximum as the envelope becomes soft (without *contrast*).

We observe that for $R \approx 1.5R_c$ we obtain asymptotically the value of $X_{max} \approx 4d$ or $4.5d$ as found before in the literature [1]. In this asymptotic regime, Kovasznay [1] observed that $X_{max} \approx 7d$ with measurements of the V_x component and Mathis [2] found that $X_{max} \approx 5d$ with measurements of the V_y as in our experiments. So in this intermediate range the behavior in this scale is reminiscent of the critical behavior of the influence length ξ in the confined hydrodynamic instabilities [3] where the Landau-Ginzburg model can explain this behavior with the law $\xi \sim (R - R_c)^{-1/2}$ as in the classical mean-field theory of phase transitions.

With this behavior in mind we proceeded to evaluate the Reynolds dependence on the amplitude of the oscillator. This evaluation has been done before [20,21,23] in order to confirm the validity of the weakly nonlinear Landau model for the evolution of perturbations. In these works the amplitude of the oscillation A, measured in a *fixed* spatial station at $x = 5d$, was plotted as a function of the Reynolds number and the law $A = A_0(R - R_c)^{1/2}$

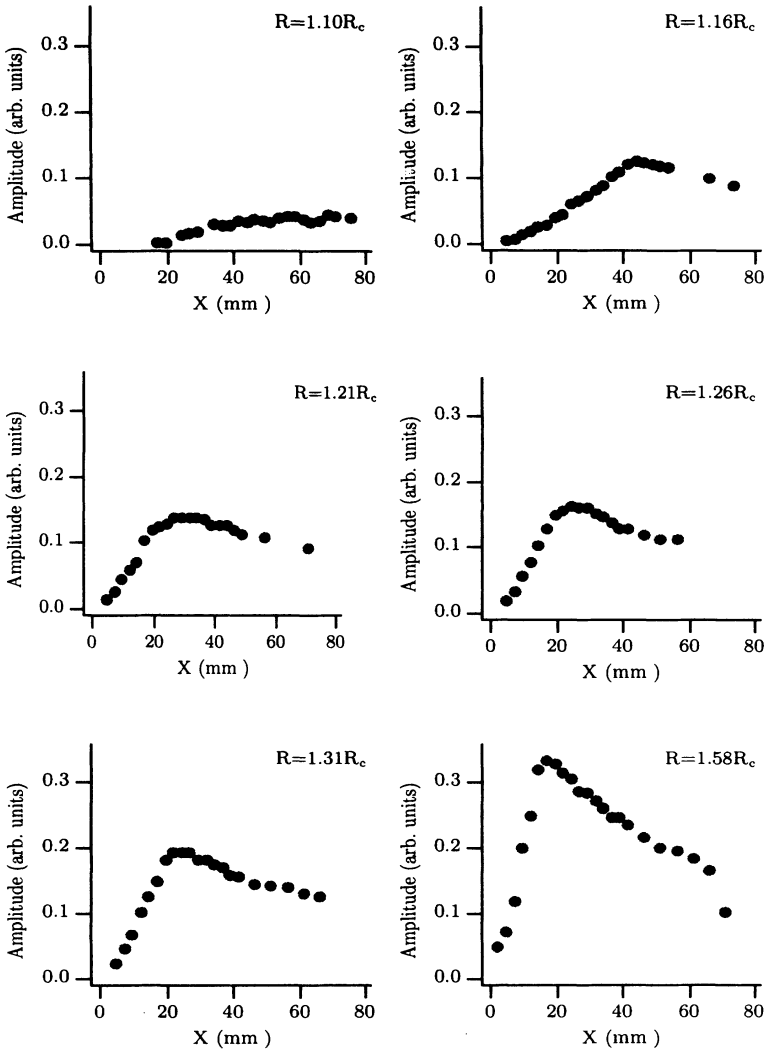

FIG. 3. Envelope of the peak to peak amplitude, in arbitrary units, for different Reynolds numbers. The abscissa x is the distance to the body in millimeters.

was obtained ($A_0 = 1/g$ is the inverse of the Landau constant). In addition, Ref. [21] claims that both the exponent 1/2 of the power law and the Landau constant do not change with x

We proceeded differently and we plotted the A_{max} value obtained from each Reynolds number measured at the point where the envelope is maximal; it is for $x = X_{max}$ and not at $x = 5d$, as has been done before. The difference can be irrelevant for $R \geq 1.5R_c$, but is more important when we approach the onset of instability. Very near this onset we are not able to ensure sufficiently good experimental precision in the localization of A_{max} and in the estimate of A_{max} as the form of the envelope is too soft. More work needs to be done in

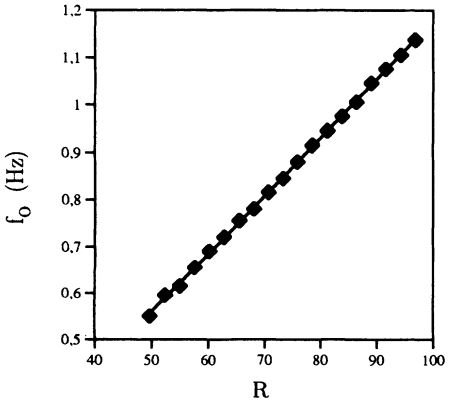

FIG. 4. Shedding frequency as function of Reynolds number.

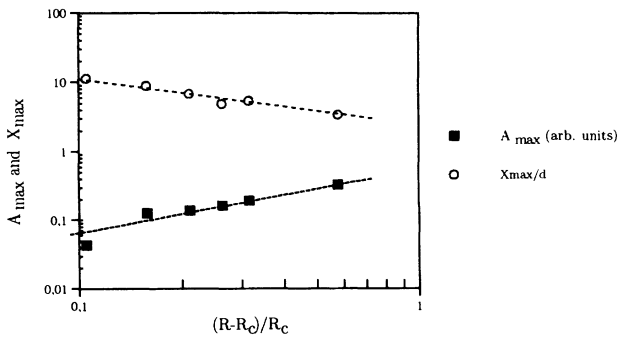

FIG. 5. Maximum amplitude A_{max} and X_{max} as a function of relative Reynolds number.

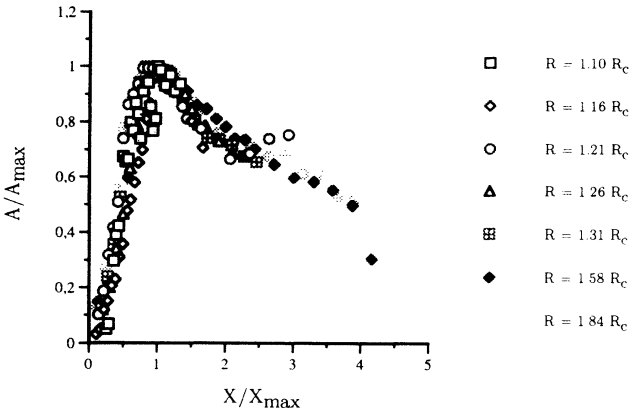

FIG. 6. Renormalized curve $\mathcal{F}(x/X_{max})$.

the future in order to reduce the experimental error in the evaluation of A_{max} when R approaches R_c.

In Fig. 5, we also show the behavior of $A_{max} = A(X_{max})$ as a function of the Reynolds number and we observe that the law $A_{max} \sim (R - R_c)$ produces a better fit. The extrapolation to zero for A_{max} gives an estimation of R_c ($R_c \approx 58$ for the smallest bluff body), very consistent with the critical value observed by the LIF flow visualization, when the streak lines of the dye begin to show the typical undulations related to the beginning of the shedding.

From the results of Fig. 5 we obtain two scaling laws for the maximal value of the perturbation and its location. From these two results we can renormalize our full results in order to incorporate these two natural scalings.

We check the validity of the assumption: $A(x, R) = A_{max}\ \mathcal{F}(x/X_{max})$, dividing each experimental value of the envelope by the maximum value A_{max} and shifting the spatial coordinate with the scale X_{max}. The renormalized full set of points corresponding to each of the experiments shown in Fig. 3 is now presented in Fig. 6. From this figure we can estimate that these two scales were fully ensuring the collapse of almost all the points of each independent measure in a universal curve for dimensionless velocity and spatial position.

IV. DISCUSSION OF THE RESULTS

In this paper we show the existence of a single curve (Fig. 6) for the renormalized amplitude of the streamwise evolution of the peak to peak amplitude of the oscillating velocity components in this instability. The crucial point in order to obtain this behavior was obtaining two scale laws related to the Reynolds number: the first one for the maximum amplitude and the second one for the position of the maximum of the global mode.

One other important aspect of our measurements was the possibility of confirming the tendency observed in the preliminary results of Mathis [2] about the scaling of the X_{max} behavior with the Reynolds number, very near the onset of instability. Many open problems are related to the physical meaning of this important spatial scale. The question is to know what is the typical length that scales X_{max}. Many scales exist in this instability and can be relevant for this problem.

(i) The amplitude of the influence length ξ_0, which scales the shift of the critical Reynolds number with the aspect ratio [3,20], is used as a prefactor of the spatial term in the Landau-Ginzburg equation.

(ii) The size of the recirculating zone behind the body and this distance is related to the shape of the bluff body. This scale is very important in the dynamic behavior in wakes to ensure the physical mechanism of feedback allowing self-sustained oscillations. Hannemann and Oertel [10] have shown the relation between the extension of the absolutely convective region behind the obstacle and the extension of the recirculating region, characterized by the negative longitudinal velocity in the central line. It is in this region that the "wave maker" acts for the entire flow [24].

(iii) The extension of the unstable region where $\varepsilon(x) \geq 0$ is related to the typical distance of the spatial inhomogeneity of the base profile of longitudinal velocity.

A series of experiments are currently in progress in order to observe these scales and identify the pertinent length which scales with X_{max}.

We also extend these experiments with measurements of the longitudinal V_x fluctuating velocity off the axis, at y_{max}. These experimental results [25] and numerical simulations of Zielinska [26] show the existence of a global mode for V_x with a larger value of X_{max} and critical exponents equal to $-1/2$ for X_{max} and equal to $1/2$ for A_{max}.

The existence of a renormalized curve for the peak to peak amplitude of the velocity fluctuation modifies the preexistent view about the pertinent order parameter of this instability. As a consequence of this we can take as a correct magnitude of the perturbation any integral measure of the velocity perturbation along the streamwise direction. If $X_{max} = X_0(R - R_c)^{\nu}$ and $A_{max} = A_0(R - R_c)^{\beta}$, the integral parameter E of the instability (for instance, the energy of one component of the velocity) becomes $E_n = \int_0^{\infty} A^n(x, R)dx \sim (A_0X_0)^n(R - R_c)^{n\beta+\nu} \int_0^{\infty} \mathcal{F}^n(x/X_{max})d(x/X_{max})$ and if this integral is constant as our results suggest, we can conclude that $E_n \sim (R - R_c)^{n\beta+\nu}$. Our results enhance the importance of the integral or global concept of order parameter in this instability.

In previous works [27,23], the evolution of the amplitude as a function of the relative Reynolds number was measured at a *fixed* position $x = x_0$. In light of our results, it implies that if this spatial station is localized between the body and the maximum of the envelope, then the form of the renormalization function $\mathcal{F}$ can be approximated with a linear function. In this case $A(x_0) = A_{max}\mathcal{F}(x_0/X_{max}) \sim A_{max}x_0/X_{max} \sim (R - R_c)^{\beta-\nu}$. So the effective critical exponent is $\beta - \nu$ and not β as was claimed. When the experiments are performed at Reynolds numbers not sufficiently close to the onset R_c , the position of X_{max} does not change significantly with the variation of R ($X_{max} \sim$ cte) and in this case $A(x_0) \sim A_{max}x_0/X_{max} \sim (R - R_c)^{\beta}$. Only in

this situation [27] the local amplitude seems to be comported as an order parameter with critical exponent β.

The form of our experimental function $\mathcal{F}$ is reminiscent of the form of the calculated function by Chomaz and co-workers [4,6], when they supposed a linear relaxation of the instability parameter $\varepsilon\ (x)$ downstream. Indeed they modeled the global mode with the Landau-Ginzburg equation

$$\tau_0 \frac{\partial A}{\partial t} = \varepsilon\ (x)(1 + \imath c_0)A + \xi_0^2(1 + \imath c_2)\ \frac{\partial^2 A}{\partial x^2} - g(1 + \imath c_1)\ |\ A\ |^2\ A,$$

taking the *linear* part of the *real* version of this equation, with $\varepsilon\ (x) = \mu_0 - \mu_1 x$. The solution with boundary conditions $A(0) = A(\infty) = 0$ is the Airy function or the parabolic cylinder function if a quadratic law was chosen for the relaxation of $\varepsilon(x)$. From the experimental point of view it is very difficult to distinguish between these functions with similar linear growth from $x = 0$, as the distinction between them occurs essentially in the tail of the curve .

In this article we show than the global mode of instability is deformed when the Reynolds number changes. This behavior has not been taken into consideration in previous theoretical studies [7,9] of the amplitude of a spatially dependent global mode.

ACKNOWLEDGMENTS

This work has been supported by a Stichting Fund. We are grateful to R. Bénard, R. Boussora, P. Deniaud, P. Ern, M. Fermigier, M. Guillaume, P. Petitjeans, and C. Tchikoo for their contribution to this experiment. The authors would like to thank S. Le Dizès s, A. Chiffaudel, P. Hebrard, M. Provansal, and B. Zielinska for fruitful discussions concerning the Bénard–Von Karman instabilities.

[1] L.S.G. Kovasznay, Proc. R. Soc. London Ser. A **198**, 174 (1949).
[2] C. Mathis, Ph.D. thesis, University of Aix-en-Provence, France, 1983.
[3] J.E. Wesfreid, Y. Pomeau, M. Dubois, C. Normand, and P. Bergé, J. Phys. (Paris) **39**, 725 (1978).
[4] J.M. Chomaz, P. Huerre, and L.G. Redekopp, Phys. Rev. Lett. **60**, 25 (1987).
[5] P. Huerre and P.A. Monkewitz, Annu. Rev. Fluid Mech. **22**, 473 (1990).
[6] J.M. Chomaz, P. Huerre, and L.G. Redekopp, in *New Trends in Nonlinear Dynamics and Pattern-Forming Phenomena*, edited by P. Coullet and P. Huerre (Plenum, New York, 1990), p. 259.
[7] P.A. Monkewitz, P. Huerre, and J.M. Chomaz, J. Fluid Mech. (unpublished).
[8] R.E. Hunt and D.G. Crighton, Proc. R. Soc. London **435**, 109 (1991).
[9] S. Le Dizès (unpublished).
[10] K. Hannemann and H. Oertel, Jr., J. Fluid Mech. **199**, 55 (1989).
[11] W. Koch, J. Sound Vib. **99**, 53 (1985).
[12] X. Yang and A. Zebib, Phys. Fluids A1 **4**, 689 (1989).
[13] *Handbook of Mathematical Functions*, edited by M. Abramowitz and I. A. Stegun (Dover, New York, 1965).
[14] A. Strzelecki, Ph.D. thesis, UPS Toulouse, France, 1989.
[15] C.H.K. Williamson, J. Fluid Mech. **206**, 579 (1989).
[16] Albarede and P.A. Monkewitz, Phys. Fluids A **10**, 744 (1992).
[17] A. Chiffaudel, Europhys. Lett. **18**, 589 (1992).
[18] A.J. Schaefer and S. Eskinazi, J. Fluid Mech. **6**, 241 (1958).
[19] F.R. Hama, Phys. Fluids. **5**, 664 (1962).
[20] M. Provansal, C. Mathis, and L. Boyer, J. Fluid Mech. **182**, 1 (1987).
[21] K.R. Sreenivasan, P.J. Strykowski, and D.J. Olinger, in *Proceedings of the Forum on Unsteady Flow Separation*, edited by K.N. Ghia (American Society for Mechanical Engineers, New York, 1987), Vol. 52, p. 1.
[22] M. Guillaume, DEA Report, University of Paris VI, 1990 (unpublished).
[23] P.J. Strykowski, Ph.D. thesis, Yale University, 1986.
[24] M.Z. Pesenson and P.A. Monkewitz, Phys. Rev. Lett. **70**, 2722 (1993).
[25] J.E. Wesfreid, S. Goujon-Durand, and P. Jenffer (unpublished).
[26] B. Zielinska (private communication).
[27] C. Mathis, M. Provansal, and L. Boyer, J. Phys. (Paris) Lett. **5**, L483 (1984).

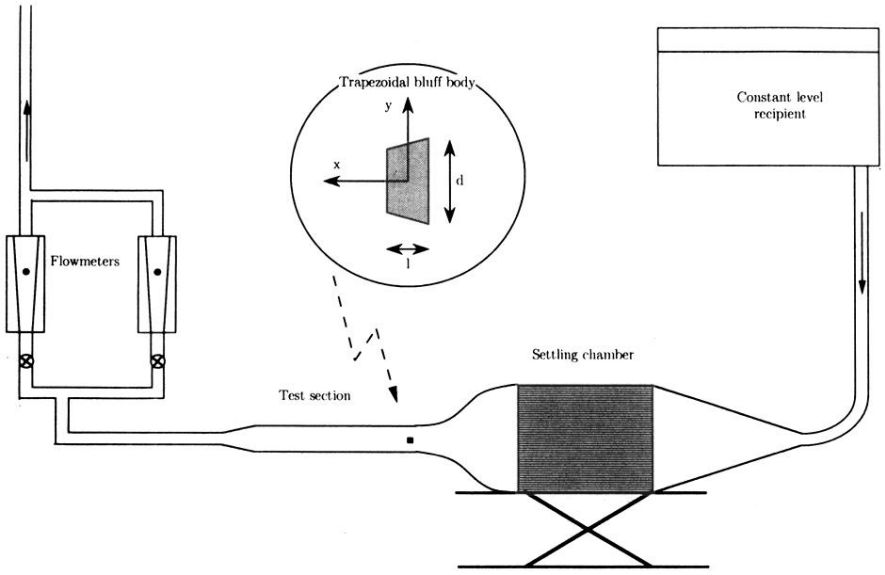

FIG. 1. Experimental setup.

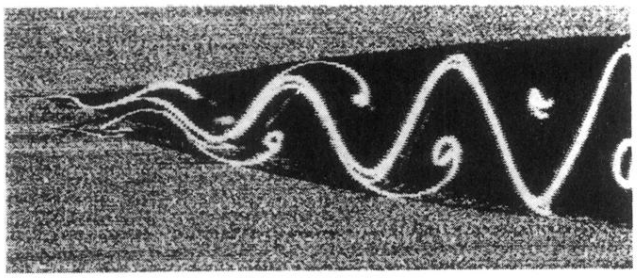

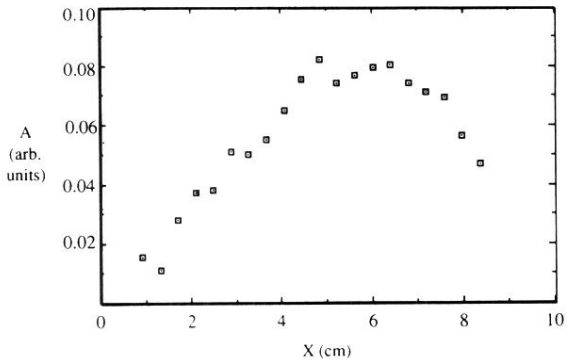

FIG. 2. (a) Laser induced fluorescence view of vortex emission. The picture shows the superposition of an instantaneous view of the streak line and the time averaged streak lines during many periods. (b) Normalized maximum amplitude of the transversal fluctuation of velocity along the x streamwise direction, measured with laser Doppler anemometry.